An overview of UAE^2 flight operations: Observations of summertime atmospheric thermodynamic and aerosol profiles of the southern Arabian Gulf

Jeffrey S. Reid,[1] Stuart J. Piketh,[2] Annette L. Walker,[1] Roelof P. Burger,[2] Kristy E. Ross,[2] Douglas L. Westphal,[1] Roelof T. Bruintjes,[3] Brent N. Holben,[4] Christina Hsu,[4] Tara L. Jensen,[3] Ralph A. Kahn,[4] Arunas P. Kuciauskas,[1] Abdulla Al Mandoos,[5] Abdulla Al Mangoosh,[5] Steven D. Miller,[6] John N. Porter,[7] Elizabeth A. Reid,[1] and Si-Chee Tsay[4]

Received 28 September 2007; revised 18 April 2008; accepted 15 May 2008; published 25 July 2008.

[1] In August through September 2004 the United Arab Emirates Unified Aerosol Experiment (UAE^2) was conducted in the southern Arabian Gulf region. We present atmospheric thermodynamic and aerosol data collected on 18 flights by the South African Aerocommander aircraft. In the first few kilometers, we observed high concentrations of both regional dust (from 100 to 300 μg m^{-3} in background, to over 1.5 mg m^{-3} in events) and ubiquitous sulfate based pollution from the Gulf's prevalent petroleum industry (10–100 μg m^{-3}). Smoke and pollution from Europe and possibly Africa were found at levels between 1.5 and 5 km. Inland, classic deep over desert boundary layer characteristics were found. Over the Arabian Gulf, dust and pollution were most often either trapped below or sequestered above a strong stable boundary. However, there were cases where a well-distributed aerosol layer crossed the inversion uniformly. Data suggest that the observed vertical profiles can be explained by the rapid formation of stable marine boundary layers as air moves offshore. This can decouple aerosol layers from within the boundary layer to those aloft in regions of vertical wind shear. In the case of pollution, the ability of flaring plumes to penetrate the inversion may also in part determine layering. In coastal regions without vertical wind shear, uniform concentrations with height across the inversion are a result of internal boundary layer development. We conclude that the bulk of the observed variability in particle vertical distribution appear to be controlled by mesoscale and microscale processes, such as the sea/land breeze.

Citation: Reid, J. S., et al. (2008), An overview of UAE^2 flight operations: Observations of summertime atmospheric thermodynamic and aerosol profiles of the southern Arabian Gulf, *J. Geophys. Res.*, *113*, D14213, doi:10.1029/2007JD009435.

1. Introduction

[2] Being the world's third largest dust source region, southwest Asia has one of the largest aerosol burdens in the world [*Middleton*, 1986; *Prospero et al.*, 2002]. With large dust events, emissions from the petrochemical industry, and transport into the region, seasonal aerosol optical thickness (AOT) are near 0.5 [*Smirnov et al.*, 2002]. Further, the Arabian Gulf (AG) littoral zone exhibits complicated meteorology, with variable sea surface temperatures (SSTs), large sensible and latent heat fluxes, and abrupt topography. However, there are very few measurements reported in the literature. The massive post–Gulf War field effort focused on burning oil well plumes. Previous studies on the more typical conditions have either focused on large synoptic patterns in the deep desert [e.g., *Ackerman and Cox*, 1989; *Rao et al.*, 2003; *Alpert et al.*, 2004], or on isolated observations of marine boundary layer (MBL) in the middle of the AG [e.g., *Brooks and Rogers*, 2000; *Atkinson et al.*, 2001]. Despite its clear importance, to our knowledge there is limited publication of combined regional aerosol and thermodynamic data.

[3] It is the complexity of the SW Asian environment which drew the United Arab Emirates Unifies Aerosol Experiment (UAE^2) to the region. In this mostly cloud free environment, researchers could work on such diverse topics as satellite and ground remote sensing, calibration and

[1]Marine Meteorology Division, Naval Research Laboratory, Monterey, California, USA.
[2]Climatology Research Group, University of Witwatersrand, Johannesburg, South Africa.
[3]National Center for Atmospheric Research, Boulder, Colorado, USA.
[4]NASA Goddard Space Flight Center, Greenbelt, Maryland, USA.
[5]Department of Atmospheric Studies, Ministry of Presidential Affairs, Abu Dhabi, United Arab Emirates.
[6]Cooperative Institute for Research in the Atmosphere, Colorado State University, Fort Collins, Colorado, USA.
[7]School of Ocean and Earth Science and Technology, University of Hawai'i, Honolulu, Hawaii, USA.

Copyright 2008 by the American Geophysical Union.
0148-0227/08/2007JD009435

validation in heterogeneous aerosol layers, dust optical properties, clear sky radiative transfer, pollution and dust microphysics, boundary layer meteorology, mesoscale dynamic, and mountain convection and precipitation.

[4] The UAE^2 study period specifically targeted the end-of-summer months. This allowed for the observation of atmospheric properties of not only the open desert and air masses transported over the AG, but also the coastal transitions between the two. At the same time, the location in the southern Arabian Gulf (SAG) allowed us to observe air masses originating from eastern Europe, the Indian Subcontinent, and possibly Africa.

[5] UAE^2 had five key assets: (1) the United Arab Emirates (UAE) Department of Water Resource Studies mesonet of 52 weather stations and 6 weather radars, (2) a mesonet of 14 strategically placed Aerosol Robotic Network (AERONET) Sun photometers, (3) the coastally sited Naval Research Laboratory (NRL) Mobile Atmospheric Aerosol and Radiation Characterization Observatory (MAARCO) super site with radiation and microphysics instrumentation, (4) the open desert situated NASA Goddard Space Flight Center (GSFC) Surface-Sensing Measurements for Atmospheric Radiative Transfer (SMART) for measuring dust optical properties near source regions, and (5) the South African Aerocommander 690A and Piper T1040 (Cheyenne II) research aircraft.

[6] In this manuscript we present general findings of the Aerocommander research aircraft of meteorological and aerosol features during UAE^2. To our knowledge, such information of meteorology coupled with particle profiles has never been reported in the literature for this region. Because this data set is so broadly utilized by the science team, this paper provides a summary of flight plans, instrumentation, and data quality. These data are then used to give an overview of the observed atmospheric state during the UAE^2 mission, including a study of how thermodynamic and aerosol features relate to the major synoptic and mesoscale flow patterns.

2. Overview of the Aerocommander Platform

[7] Although the UAE^2 study was conducted from 4 August to 5 October 2004, aircraft operations were performed only during the second half of the study, from 27 August through 5 October. The primary platform was the South African Meteorological Service Aerocommander 690A, contracted by the University of Witwatersrand. On occasion, state variable data were also collected by the Orsmond Aviation Piper T1040 (or Cheyenne II; similar to a Cheyenne) also contracted by the University of Witwatersrand. More descriptions of both aircraft are provided in Appendix A.

[8] In this paper we focus on state thermodynamic variables and profiles of fine and coarse mode particles. Thermodynamic measurements were made with Rosemont temperature and pressure instruments and an EGG dew point hygrometer. Particle measurements were made with a Passive Cavity Aerosol Spectrometer Probe (PCASP) and Forward Scattering Spectrometer Probes (FSSP). For this study, we followed the measurement guidelines laid out by *Reid et al.* [2003b]. For distributions of fine particles, we relied on the PCASP (diameter 0.1–3 μm). With the deicing heaters on, the size distributions from the PCASP should be considered dry [*Strapp et al.*, 1992; *Reid et al.*, 2006]. To estimate fine mode mass we integrated between 0.1 and 0.6 μm and assumed particles were primarily ammonium sulfate internally mixed with black carbon (K. E. Ross et al., Fine mode aerosol particles in the southern Arabian Gulf and United Arab Emirates, manuscript in preparation, 2008). Values used for index of refraction and density, and for single scattering albedo were n = 1.53–0.01i and ρ = 1.77 g cm^{-3}, ω_o = 0.95, respectively.

[9] While the PCASP has long been proved efficacious for measuring fine mode particles, for the coarse mode, the FSSP instrument suffers from significant response function degeneracy issues that result in over sizing [*Reid et al.*, 2003a, 2006]. This produces volume distributions centered around 8–10 μm in diameter, regardless of the input particle size spectrum. Hence, the FSSP can functionally differentiate changes in size and particle concentration only semi-quantitatively. Despite these drawbacks, the FSSP is useful if applied properly, such as described below.

[10] To estimate coarse mode mass and the relative vertical distribution of dust, we took advantage of the FSSP's ability to correlate column integrated coarse mode volume, or cross-sectional area, with optical depth [*Reid et al.*, 2003b]. For most flights, the FSSP was set to gain level 2 (0.7–19 μm), but on four occasions, the gains were changed in flight: three times to gain level 0 (1–38 μm, on 29 and 30 September and 1 October) and once to gain level 3 (0.5–8 μm on 12 September). Also, the FSSP was not installed on the first few flights, so the coarse mode mass was correlated to the last channels in the PCASP. To account for these variations in FSSP configuration we cannot simply correlate vertically integrated cross-sectional area with optical depth. To ensure uniformity, voltage data for the size range between 1 and 3 μm were used for both the FSSP and PCASP. Further, by limiting the range to 3 μm, we not only account for most of the dust's light scattering but also avoid the size regime where the FSSP is known to oversize particles [*Reid et al.*, 2003a, 2006]. We also had the advantage during the UAE^2 mission of being able to apply the *O'Neill et al.* [2001] spectral deconvolution method for separating fine and coarse mode optical depth to the AERONET AOT spectrum, thus removing ambiguity between fine and coarse mode particle amounts. In Figure 1 we show the comparison between the FSSP column-integrated indicated volume in the 1–3 μm range to AERONET coarse mode AOT at 675 nm. As in the Puerto Rico Dust Experiment [*Reid et al.*, 2003b], the correlation is excellent (r = 0.98 and 0.97 for the FSSP and PCASP, respectively). This regression is from 12 complete profiles from 12 separate flights and thus we have confidence in the relationship. For our vertical profile comparisons we utilize this regression to estimate dust mass load by assuming a dust mass extinction efficiency of 0.4 m^2 g^{-1} (as calculated at the MAARCO site during the mission). Because hygroscopic sea salt is such a small fraction of the coarse mode mass [*Reid et al.*, 2008], it is likely that this approximation holds for both dry and humid conditions.

[11] As also seen in Figure 1, the cross correlation between the FSSP and PCASP had a correlation coefficient of 0.96 but with a slope of 0.5. This indicates that the last channels in the PCASP also correlated well with column

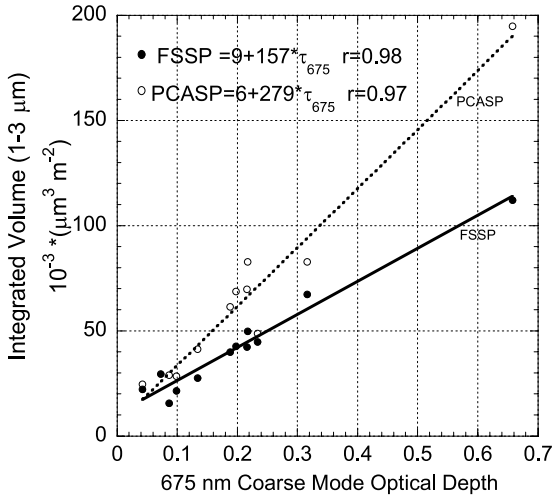

Figure 1. Correlation of FSSP-100 aerosol volume in the 1–3 μm range to the 675 nm coarse mode optical depth derived from applying the *O'Neill et al.* [2001] spectral deconvolution to AERONET data.

optical depth (although not quite as robustly as with the FSSP). The low slope is expected because the FSSP is known to underestimate particle concentrations in the lowest channels [*Reid et al.*, 2006]. To ensure uniformity for cases where the coarse mode was inferred from the PCASP instead of the FSSP, we apply the same technique for determining dust mass. Namely, correlate the volume with AOT and use a mass extinction efficiency of 0.4 m^2 g^{-1}.

[12] It is important to emphasize that this approach is taken so flight results can be compared; we are not attempting any form of "closure." Indeed, given the current state of the art, the "column closure" approach for coarse mode particles such as dust is problematic [*Reid et al.*, 2006]. Rather, we compare the relative vertical profiles of fine and coarse mode particles under different regional meteorological conditions. In our opinion, this data processing approach suffices for our current purpose.

3. Flight Plans and Mission Summaries

[13] Summaries of the UAE^2 mission flights and tracks are presented in Table 1 and Figure 2, respectively. Because the 690A was not equipped with its own Sun photometer, most flights were performed in the vicinity of AERONET sites [*Eck et al.*, 2008]. Flights occurred between 27 August and 5 October and included a variety of flight plan features such as satellite calibration and validation, radiation, studies of meteorological coastal transitions, and the land and sea breezes. Underflights were flown to support the satellite sensors on Terra (Multiangle Imaging Spectroradiometer (MISR), Moderate Resolution Imaging Spectroradiometer (MODIS), Clouds and the Earth's Energy System (CERES)), Aqua (MODIS), Sea-viewing Wide Field-of-view Sensor SeaWiFS, and Advanced Very High Resolution Radiometer (AVHRR), with MISR receiving the highest priority. On special occasions underflights were flown for EO-1 Hyperion, Advanced Spaceborne Thermal Emission and Reflection Radiometer (ASTER) and Quickbird. On one occasion, 28 September, the 690A and Piper T1040 flew in formation.

[14] Most aircraft flights were performed during the morning hours to support Terra and occasionally SeaWiFS. Missions mostly took the form of simple descending vertical profiles over key AERONET sites from ~500 hPa (6 km) to the surface. The favored targets for this work were the AERONET sites at Hamim (on the border of several Aeolian features), the coastal MAARCO site and the over-

Table 1. Flight Summaries for the Aerocommander 690A[a]

Flight	Flight Plan	Target Regions	Source Region	Takeoff (UTC)	Land (UTC)	Satellites	500 nm AOT	η
20040827A	TF	AD	EQ/Y	1244	1343	–	0.48	0.23
20040828A	SP	SM	EQ/Y	1224	1456	–	0.38	0.31
20040830A	SP, CT	MA	NG/I	0701	1022	S, MA	0.62	0.72
20040901A	SP	DE, MA	NG/I	0459	0838	MR	0.36, 0.65	0.54, 0.69
20040903A	SP	MA	UAE	0425	0605	A, MCT	0.49	0.33
20040907A	SP, CT	MA, SN	EQ/Y	0445	0830	–	0.59, 0.64	0.28, 0.31
20040908A	SP, CT	MA, SN	EQ/Y	0722	1039	–	0.40, 0.38	0.31, 0.38
20040910A	SP	HA	UAE	0413	0755	MR, MCT	0.29	0.36
20040912A	SP	GOO	IN/P	0433	0834	MR	cloudy	–
20040912B	SP	MA	NG/I	0934	1113	MA	0.9	0.27
20040913A	SP	MA	NG/I	0638	0758	S	0.42	0.43
20040928A[b]	SP	HA, MA	UAE	0345	0704	MR, MCT, EO1, S	0.29, 0.32	0.33, 0.35
20040929A	SB, CT	MA, SN	UAE	0345	0705	MCT, S, QB	0.29, 0.24	0.37, 0.41
20040929B	SP	MA	UAE	1031	1335	MA, AV	0.25	–
20040930A	SB, CT	SN; SM	UAE	0808	1232	S, MA	0.22, 0.16	0.43, 0.35
20041001A	SP	HA	CG/UAE	0321	0721	MCT	0.17	0.40
20041002A	SB, CT	SN; SM	NG/I	1140	1426	MA, AV	0.58	0.85, 0.56
20041002B	SB, CT	SM, coast	NG/I	1511	1620	–	–	–
20041003A	SP, P	AB	NG/I	0449	0900	MR	0.28	0.62
20041005A	SP	SN	NG/I	0458	0723	MCT	–	–
20041005B	SP	SN, AD	NG/I	0800	0927	MCT	–	–

[a]Given is the flight number (YYYYMMDDn), flight plan (TF, test flight; SP, simple profile; CT, coastal transition; SB, sea breeze; P, plume) and the target regions (primary followed by secondary, MA, MAARCO; SM, SMART; HA, Hamim; SN, Sir bu Nair; AB, Abu al bu Khoosh; AD, Abu Dhabi; AK, Al Khaznah; DE, Delma; GOO, Gulf of Oman). Also given is the primary source region for the air mass sampled (EQ/Y, empty quarter/Yemen; NG/I, northern Arabian Gulf/Iraq; UAE, United Arab Emirates; IN/P, India and Pakistan; CG, central Arabian Gulf). Takeoff and landing times given in UTC. Satellites indicate satellites supported (AS, ASTER; AV, AVHRR; EO1, EO1/Hyperion; MA, MODIS on Aqua; MCT, MODIS and CERES on Terra; MR, MISR; QB, Quickbird; S, SeaWiFs).

[b]Flight coordinated with Piper T1040.

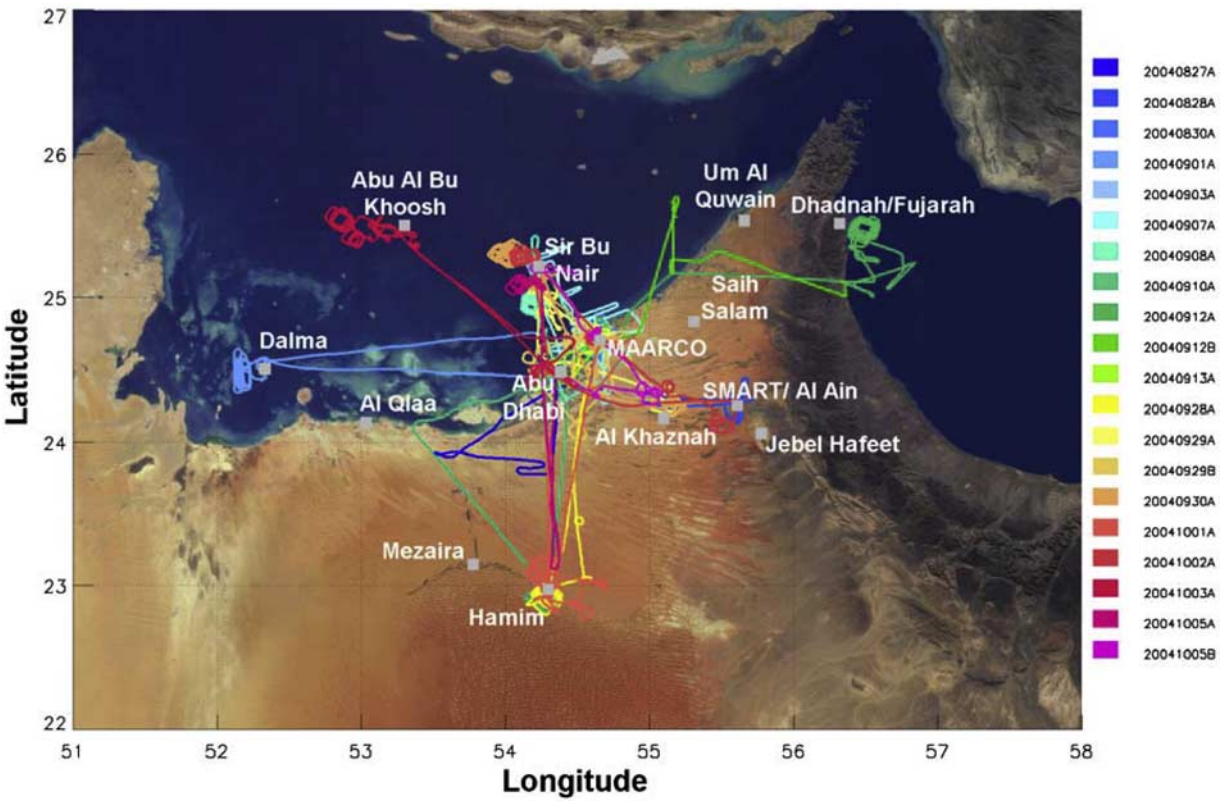

Figure 2. Flight tracks of the Aerocommander 690A missions during UAE^2. AERONET sites are marked with gray boxes. Background from a MISR regional composite (courtesy of Jim Knighton, Glendale College, California).

water site at Sir bu Nair Island. UAE Air Force activities prevented morning overflights of the SMART site at Al Ain. Special flights to Delma Island and Dhadnah were conducted to support MISR. To study mesoscale phenomena, the 690A flew transects exploring the coastal transition of the sea and land breeze circulations including vertical profiles up to the 700 hPa level.

[15] On the basis of the analysis of *Reid et al.* [2008], the operations area was impacted by aerosol particles from at least four diverse source regions: (1) pollution from coastal and offshore oil processing facilities and dust from the northern Gulf region, such as the Tigris-Euphrates basin in Iraq; (2) dust transported from Oman/Yemen as well as UAE coastal carbonate deposits; (3) regional dust from sources within the UAE; and (4) dust from the northern UAE and southern Iran. The first three phenomena were observed during the research flights (Table 1).

[16] Optical depths varied significantly during the mission, with midvisible AERONET-derived values ranging from 0.2 to 0.8 at MAARCO [*Eck et al.*, 2008]. The fine-mode fraction (η) of the AOT varied from about 0.25 to 0.8. This variability was observed during the flights with profile AOTs ranging from 0.17 to 0.9 and fine-mode fraction ranging from about 0.25 to 0.85 (Table 1).

4. Large-Scale Aerosol Features Over the Southern Arabian Gulf

[17] Full profiles of aerosol and thermodynamic properties conducted during the mission can be broadly placed into three categories: (1) inland desert, (2) over water (southern Arabian Gulf (SAG)) with large-scale northwesterly onshore flow, and (3) over water SAG with large-scale southwesterly offshore flow. Summaries of vertical profiles of state variables and inferred aerosol concentrations for these three categories are presented in Figures 3, 4, and 5, respectively. Included are temperature, T; dew point, T_d; equivalent potential temperature, θ_e; relative humidity, RH; water vapor mixing ratio, ω_v; and fine and coarse mode particle concentrations (discussed in section 2 and deduced from Figure 1). It is emphasized that the derived FSSP mass is an optical equivalent mass and is used for simple flight-to-flight comparison purposes.

4.1. Inland Desert Profiles

[18] During the UAE^2 mission four full profiles were performed at inland desert sites: Once at the SMART site in the midafternoon (1500 LST on 28 August), and three at the Hamim site at midmorning (1000 LST on 10 and 28 September and on 1 October). For comparison purposes, one afternoon (SMART, 28 August) and one morning (Hamim, 10 September) profile are presented in Figure 3. In these cases, background fine mode/pollution particle concentrations tend to be low (<5 μg m^{-3}). An elevated pollution plume is present at 1600 m over Hamim. For the afternoon case dust concentrations increase and decrease 20–40 μg m^{-3} every 200 m through the depth of the profile.

[19] The temperature profiles exhibit classic over-desert boundary layers [*Warner*, 2004], and are similar to the

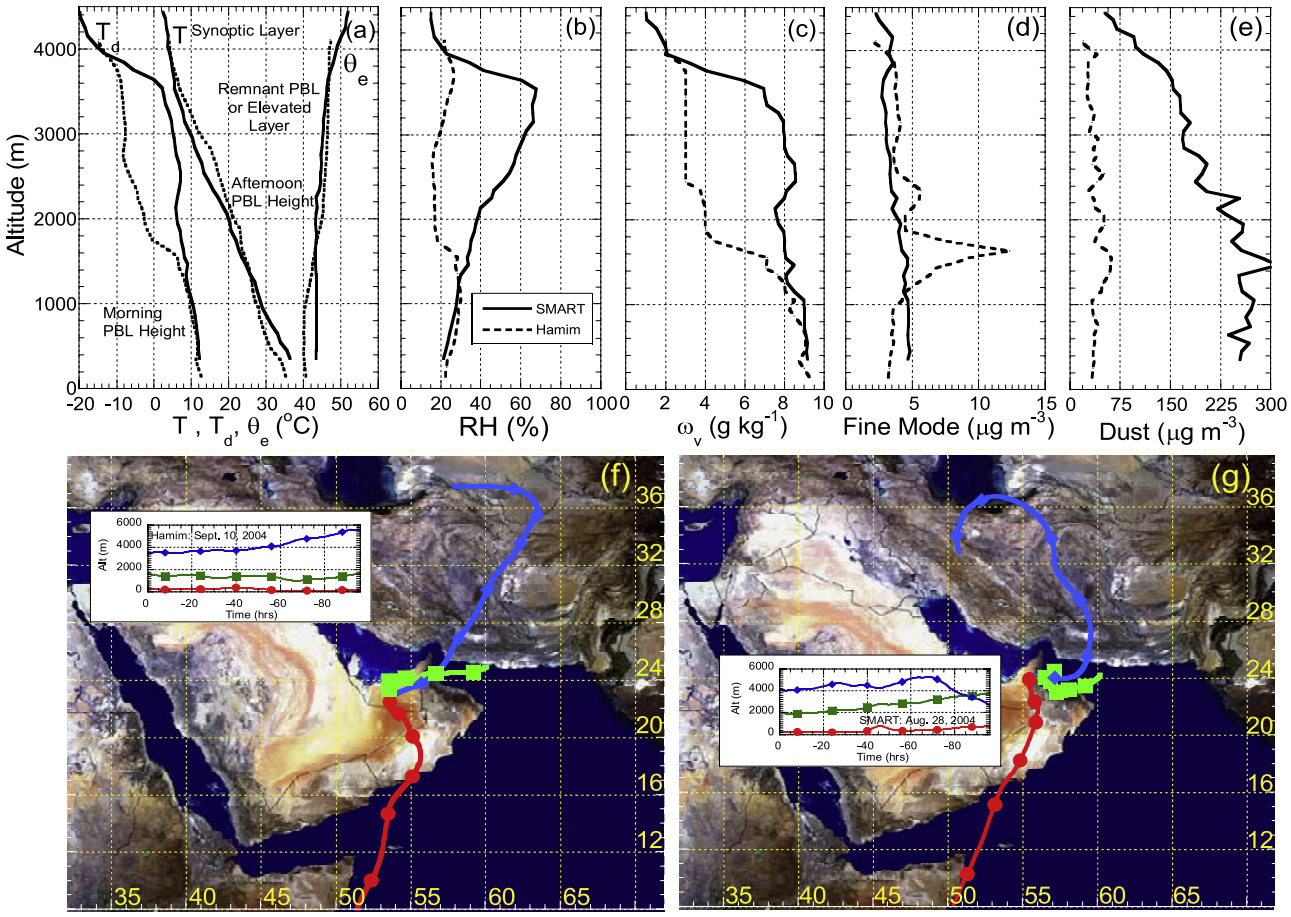

Figure 3. Boundary layer profiles over the SMART site the afternoon of 28 August 2004 and Hamim for the morning of 10 September 2004. Included are (a) atmospheric state variables temperature (T, °C) dew point (T_d, °C), and equivalent potential temperature (θ_e, °C); (b) relative humidity; (c) water vapor mixing ratio (g kg^{-1}); (d) estimated dry fine mode mass concentration (μg m^{-1}); (e) estimated dust mass concentration, (μg m^{-1}); (f) 96 h HYSPLIT back trajectories for the 10 September case from significant feature levels with major tick every 6 h, start at 200 m level (red), 1800 m level (green), and 3800 m level (blue); and (g) same as Figure 3f for the 28 August case but start at 200 m (red), 2000 m (green), and 4000 m (blue).

findings of *Ackerman and Cox* [1982] in central Saudi Arabia. The planetary boundary layer (PBL) is well mixed from the surface to the base of the inversion at 1000 m for the morning case (typical for all three morning profiles), and higher at 2200 m in the afternoon profile (observable in both the θ_e and ω_v profiles). Intermediate layers are present between the PBL inversion and the subtropical subsidence inversion, measured at 3800 to 5000 m during the mission. On the basis of HYSPLIT [*Draxler and Hess*, 1997] back trajectories, significant vertical wind shear was present. Lower boundary layer air (<1000 m) was advected from the south over Oman and the Arabian Sea, while upper air (>2000 m) came from the northeast, passing from the Gulf of Oman (GOO), central Iran and western Asia (Figure 3f). At the pollution plume level, HYSPLIT suggests the logical origin of the pollution plume to be the prevalent petrochemical industry in Abu Dhabi and the SAG. As the PBL builds during the day, this layer would likely be eroded into the main PBL.

[20] For the afternoon profile over the SMART site, the somewhat moister layer between 2000 and 3800 m (also identifiable in θ_e and ω_v profiles) may be a remnant of a previous day's warmer and deeper boundary layer (in this case >3 km in depth, which is not unreasonable [*Warner*, 2004; *Warner and Sheu*, 2000]). On the subsequent day, if the boundary layer height does not reach the same altitude, the top of the layer and inversion can persist. From HYSPLIT (Figure 3g), air at 4000 m flowed over Iran and the GOO with lower-level air originating from the south (similar to the morning case). Midlevel air appears to be regionally stagnant.

4.2. SAG During Northwesterly (NW) Onshore Flow Conditions

[21] While more thorough studies of the interior desert data in UAE[2] are being analyzed, in this manuscript, the focus is more toward the SAG itself, and especially the coastal transition. During the Monsoon season (June–September), there are typically dust laden northwesterly winds of 5–10 m s^{-1} that prevail across Iraq and the AG, known as the summer or 40 day Shamal (after the Arabian word for north) [*Rao et al.*, 2003]. These winds are strongest

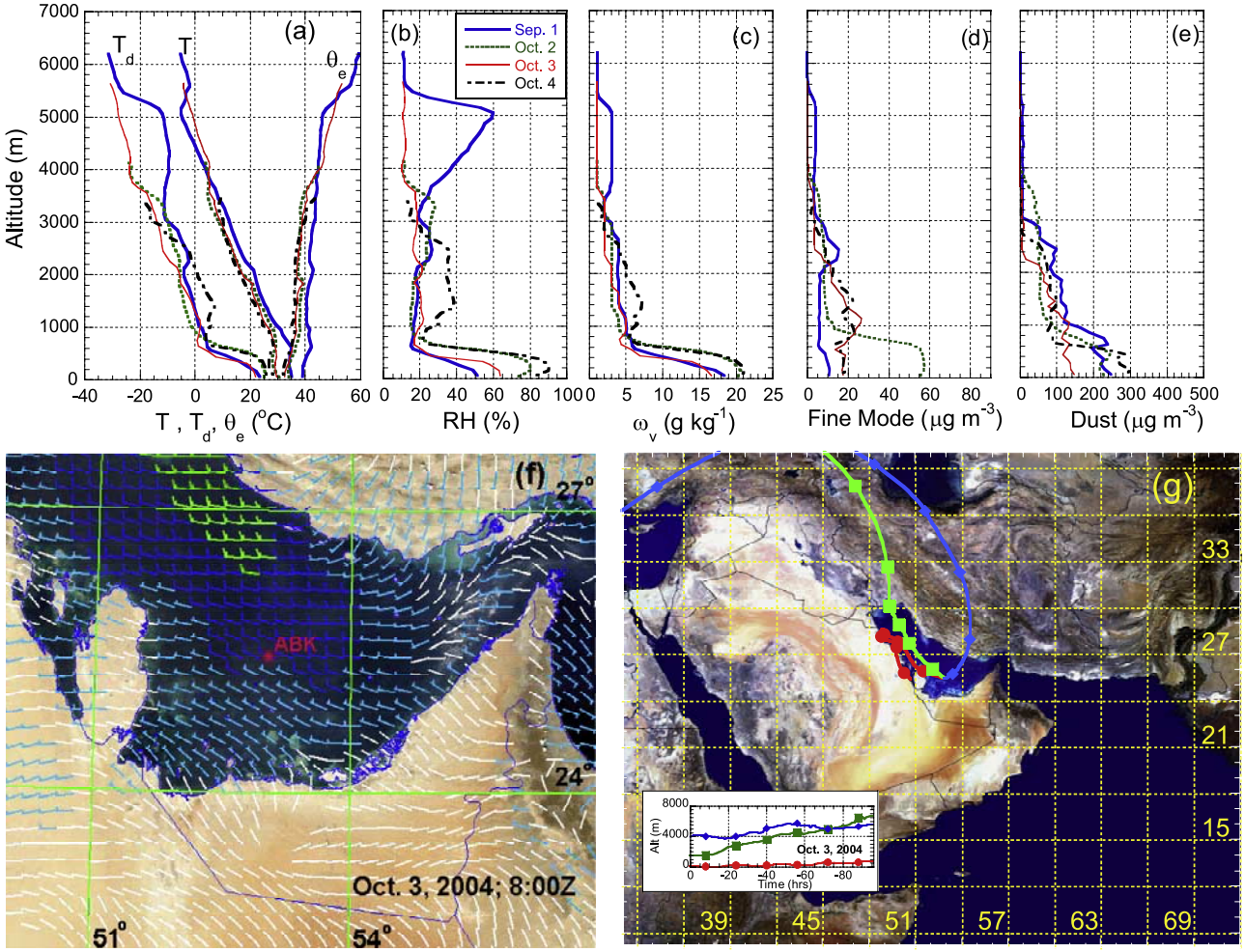

Figure 4. Onshore or shoreline profiles for periods of typical northwesterly synoptic forcing of 1 September and 2, 3, and 5 October. (a–e) Same as Figure 3 and (f) MODIS Terra satellite RGB images with COAMPS® surface wind fields for 3 October for the Abu al bu Khoosh profile (marked ABK). Long barbs are 5 m s^{-1}, and short barbs are 2.5 m s^{-1}. (g) HYSPLIT back trajectories from significant levels for 3 October 2004 from Abu al bu Khoosh (red 100 m, green 1500 m, and blue 4000 m, major tick every 6 h).

in June and July, and are a result of interactions between the Saudi Arabian high and the Indian monsoonal trough, with a deeper trough forcing stronger northwesterly winds [*Heishman*, 1999]. Hence, while typically sustained in midsummer, by September and October the NW winds can weaken or reverse [*Rao et al.*, 2003].

[22] On the basis of the combined trajectory and chemistry analysis of *Reid et al.* [2008] during the August–September time period, the SAG was impacted by significant northwest flows carrying dust from the Iraq/NAG region on 11, 12, 15, 30, and 31 August and 1, 12, 15, 16, 25, and 26 September, including a significant Shamal dust event on 12 September. Further meteorology and satellite analyses in the region suggest that the SAG remained under the NW flow from 1 to 5 October. Flights occurred on 30 August and 1 and 12 September, and 2, 3, and 5 October for this wind flow regime.

[23] Figure 4 presents atmospheric state variables and aerosol concentrations for four vertical profiles over the SAG during NW flow conditions: 1 September over Delma Island; 2 October over Sir bu Nair Island; 3 October over Abu al bu Khoosh; and 5 October over Sir bu Nair Island, (see Figure 2). The 30 August and 12 September flights are discussed as case studies in section 5.

[24] Profiles were characterized by layer regimes marked by three key inversions. As in the open desert cases, we have the expected 4000–5000 m (~650–500 hPa) extremely dry (ω_v < 1 g kg^{-1}) subtropical subsidence inversion associated with the downward motion of the Hadley Circulation. At the bottom of the atmosphere, there is a marine boundary layer (MBL) inversion at 500 to 800 m (~950 hPa) above sea level, capping a stable and moist MBL. These MBLs are clearly identifiable in the θ_e and moisture profiles. RH values near the surface were on the order of 60 to 90%, corresponding to ω_v from 18 to 23 g kg^{-1}. Last, at least one more inversion was typically present at 1000–3000 m (900–700 hPa). Given that the AG is essentially an inland sea surrounded by deserts, this regime is likely remnants of an upwind desert planetary boundary layer.

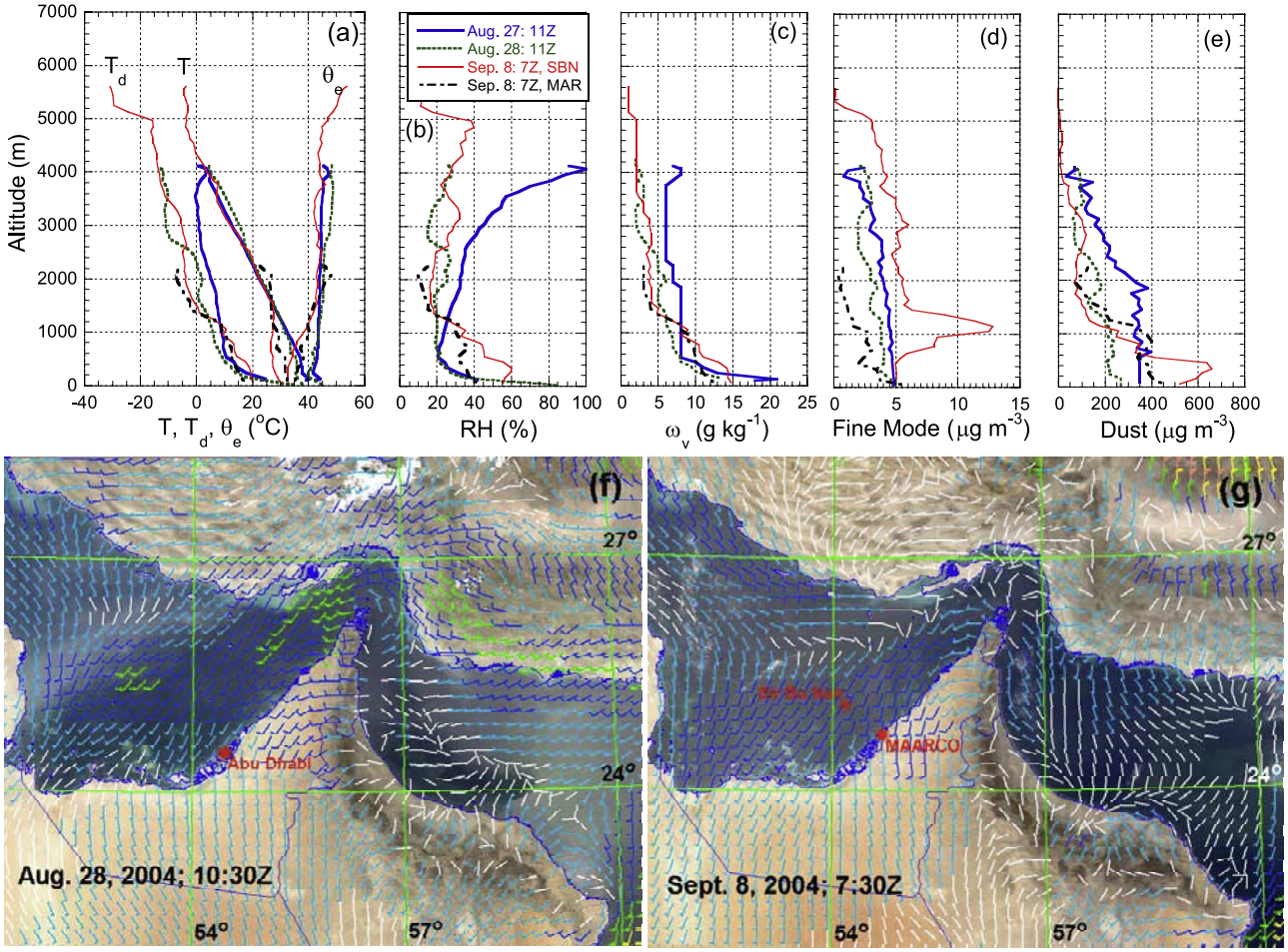

Figure 5. Offshore or shoreline profiles for periods of southwesterly synoptic forcing: (a) atmospheric state variables, (b) relative humidity, (c) water vapor mixing ratio, (d) estimated dry fine mode mass concentration, (e) estimated dust mass concentration, and (f and g) MODIS Terra satellite RGB images with COAMPS® surface wind fields. Long barbs are 5 m s^{-1}, and short barbs are 2.5 m s^{-1}. Key landmarks have been annotated in red to show location of vertical profiles. Profiles on 8 September were 20 min apart.

[25] Flow patterns for these cases can be seen in the mesoscale Coupled Ocean Atmosphere Mesoscale Prediction System (COAMPS®) (COAMPS® is a registered trademark of the United States Naval Research Laboratory) midday flow pattern overlaid on the MODIS Aqua RGB image for the 3 October 2004 flight in Figure 4f (see *Eager et al.* [2007] for complete details on the COAMPS® performance for the UAE^2 mission). The COAMPS® simulations follow the climatology assessment of *Heishman* [1999] and hence we treat this case as typical. As the NW winds flow down the AG, they are modified by the Zagros Mountains in Iran and the Al Hajar Mountains on the Omani Peninsula. Over the water east of Doha (Qatar), the terrain acts to "turn" the winds from northwesterly to westerly and finally southwesterly as one approaches the Strait of Hormuz. On the Iranian side of the SAG, winds are frequently southeasterly and easterly. In the GOO, the strength of the easterly winds is positively correlated to the AG NW flow via the Indian Monson, resulting in convergence of the wind in the Strait of Hormuz and along the windward side of the Al Hajar Mountains. In addition, land/sea breeze circulations (LSBC) modify this wind regime for coastal and inland sites around the entire AG, including the UAE [*Zhu and Atkinson*, 2004; *Eager et al.*, 2008]. READY HYSPLIT back trajectories for the 3 October case (Figure 4g) show that at the lowest levels, winds were from the WNW, while just above the MBL inversion, the winds were from the NW and could be traced back to eastern Europe.

[26] For nearly all of our SAG flights in NW flow conditions, these flow patterns were similar, and consequently MBL properties were similar. The exception is the flight of 1 September over Delma Island in the western SAG (Figure 2). The MBL sampled over Delma Island had a lower height and water vapor mixing ratios. Wind analysis shows for the other flights, sampled air masses had spent ~10 h or traveled 100 km over the AG resulting in a more developed MBL than the 1 September flight.

[27] All of the thermodynamic boundary layer observations presented in Figure 4 are similar to the mid-AG reports from a midspring data collect presented by *Brooks and Rogers* [2000], although they found lower boundary layer tops (100–200 m). From numerical simulations [*Atkinson et al.*, 2001] it was suggested that within 48 h (after placing

the air mass in the SAG) the MBL would reach 500 m, similar to our findings.

[28] Unique to the UAE^2 campaign was the additional observation of aerosol particle properties relative to thermodynamic soundings. Estimated fine and coarse mode profiles are presented in Figures 4d and 4e. We found that in most cases the MBL inversion provided a boundary between dust and pollution layers, with occasional elevated plumes aloft.

[29] The MBL most often had the highest pollution concentrations, typically ranging from 10 to 60 μg m^{-3}; in one case reaching 100 μg m^{-3} (see discussion in section 5). Two instances where peak pollution (fine mode) concentrations of 25 and 22 μg m^{-3} occurred above the MBL inversion are 3 or 4 October (Figure 4d). This variability in pollution vertical distribution appears to be linked to whether or not individual gas flare plumes had the buoyancy to penetrated the MBL inversion. Physical observations and further details of flare penetration will be presented in an upcoming paper by Stuart Piketh et al. Last, regarding fine mode particles, in the case of 1 September we did observe a significant plume at 2500 m. HYSPLIT back trajectories had this air mass passing from a biomass burning plume region in Africa and looping over northern Saudi Arabia. While this is suggestive of a biomass burning origin, the 2500 m altitude is within typical Saudi boundary layer heights, and this may be a PBL remnant layer originating from Saudi urban pollution or petroleum activities.

[30] Dust (coarse mode) tended to behave similar to pollution, but with a greater propensity for high concentration in the MBL rather than aloft. Concentrations ranged from 150 to 300 μg m^{-3} for typical NW wind conditions, but reached 1500 μg m^{-3} for the 12 September Shamal event (see section 5). Unlike pollution, on several occasions (such as 3 October), dust concentrations above and below the MBL inversion were similar. Dust also had a tendency to reach higher altitudes than pollution, from 2200 to 3800 m with concentrations above 50 μg m^{-3}. This finding is consistent with our interior desert observations and leads to the following hypothesis. Dust is mobilized over the desert and mixed throughout the PBL to the height of 3 km or more. Once the air mass is advected over the AG, this dust laden layer is then decoupled from the surface through the formation of the MBL. In the next section we explore the decoupling by observations of large-scale offshore flow.

4.3. SAG During Southwesterly (SW) Offshore Flow Conditions

[31] Even though the summer months tend to be dominated by NW winds, at times the coupled high pressure to the north and Indian monsoonal trough near the Arabian Sea weaken, resulting in large-scale southwesterly flow, and offshore flow from the UAE into the SAG. Similar to the chemical and trajectory analyses for NW flow conditions, *Reid et al.* [2008] indicated large-scale SW winds on 22–29 August and 2, 3, 7, and 8 September 2004. For these cases, dust chemical composition included carbonates from deposits along the UAE coast (2 and 8 September) as well as similar enrichment from beds in Oman and Yemen (23–28 August).

[32] Four representative thermodynamic and aerosol particle soundings at or near the UAE coast, taken from three flights on 27 and 28 August and 8 September, are presented in Figures 5a–5e in a format similar to Figure 4. COAMPS® surface winds overlaid on MODIS RGB images are shown for 28 August and 8 September in Figures 6f and 6g, respectively. Back trajectories for all of the SW flow conditions are given by *Reid et al.* [2008]. From these back trajectories the air passed over the southern UAE from Oman or Yemen, and possibly originating in the Somali Jet of Africa.

[33] Through comparison of COAMPS® flows in Figures 4f and 5f, significant differences can be seen between the two flow regimes in the SAG. Following *Heishman* [1999] for the SW wind flow regime: (1) Air masses move out of the UAE into the SAG with a counterclockwise motion; (2) the air splits in the SAG, with flow divergence into the central AG and Strait of Hormuz; and (3) the typical easterly winds in the GOO reverse and become westerlies or weaken and stagnate.

[34] The 27 and 28 August cases flights were conducted in midafternoon LST, just offshore the UAE coast. Profiles show typical afternoon soundings for subtropical or interior desert regions, as observed in section 4.1. The subtropical subsidence inversion capped the profiles (at 4,000 m, 650 hPa). On the basis of the θ_e, ω_v and particle profiles, however, we estimate the original PBL moving offshore was at ~2 km. On 27 August, midlevel moisture was advected from the east with a thin cloud deck at 4000 m. Given that the profiles were taken just offshore over warm SAG water (>30°C), the influence of latent heat fluxes on the temperature and moisture variables is seen in Figures 5a–5c resulting in an internal boundary layer in the lowest 100–200 m.

[35] For both fine and coarse mode aerosol particles for 27 and 28 August, concentrations varied by roughly a factor of two. Fine mode maximum concentrations of 5 μg m^{-3} and 200–300 μg m^{-3}, for particles and dust, respectively. Concentrations correlate with changes in ω_v, indicating a change of air mass. Within the desert PBL (2 km), particles are clearly well mixed. In Figure 5e an elevated dust layer is seen between 1600 and 2600 m for 28 August. As we would expect, the development of over water internal boundary l3ayers as the parcel moves over the AG does not significantly impact near surface particle profiles in this case. As no significant aerosol particle sources or sinks exist over the water in this region, the afternoon internal boundary layer would develop without correlation to aerosol vertical profile.

[36] The flights on 8 September, demonstrate how profiles can change over relatively short distances in the littoral zone. The 8 September flights occurred during the late morning from 1022 to 1339 LST. One full profile was taken 80 km offshore near Sir bu Nair Island, and a partial profile was acquired over the coastal MAARCO site which initiated 20 min later (Figure 5g). As sampled over MAARCO, the boundary layer height was 1.2 km with low fine mode particle concentrations of 5 μg m^{-3}. Dust concentrations were high ~400 μg m^{-3} and remained constant through the depth of the boundary layer. A rapid decrease in dust concentrations was seen above this layer. Such an aerosol profile reflects the desert origins of the air mass in a developing morning boundary layer.

[37] Dramatic differences are evident when we compare the Sir bu Nair Island and MAARCO profiles for 8 September.

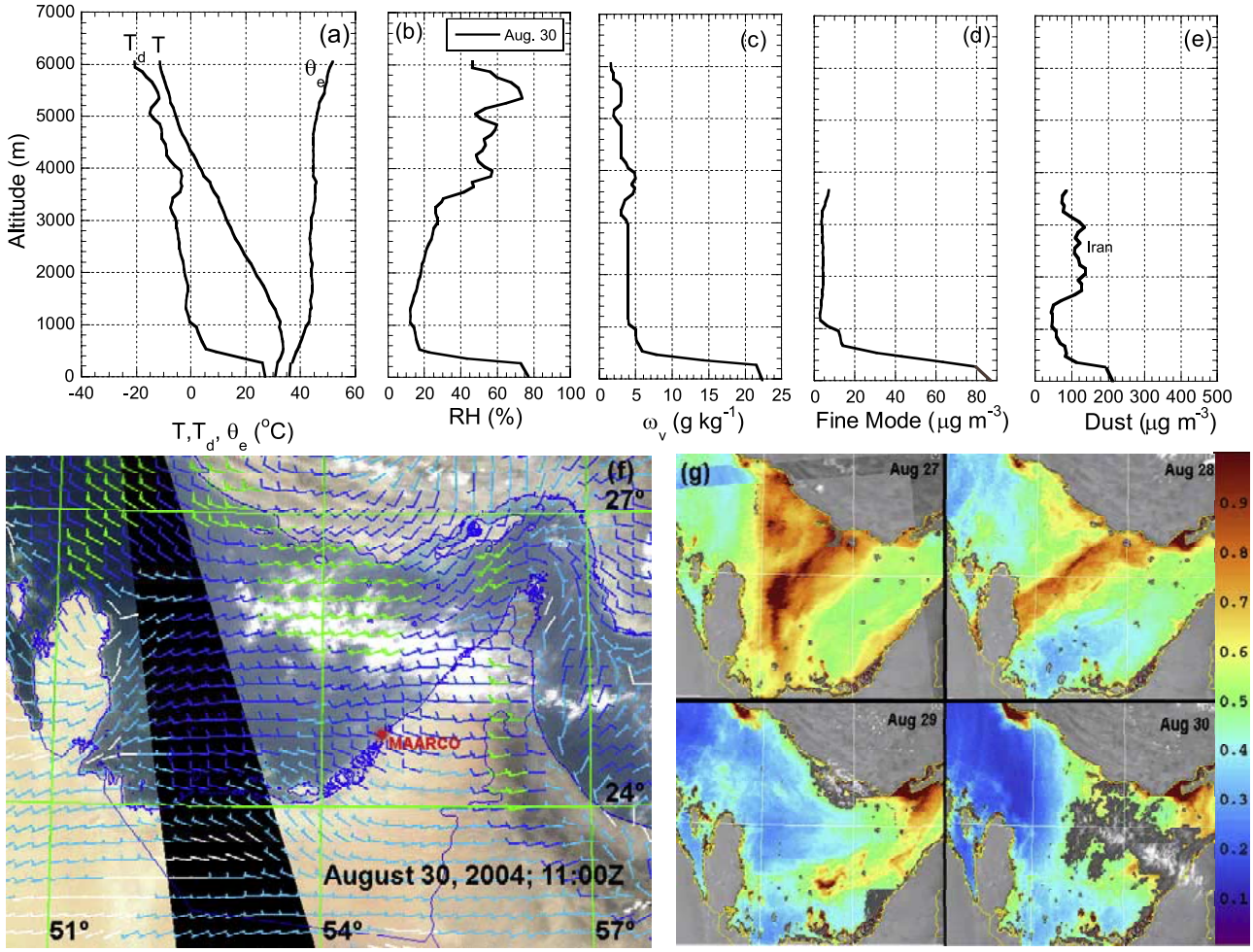

Figure 6. (a–f) Same format as Figure 7 for the air pollution event of 30 August 2004. (g) Daily time series of MODIS 1 km optical depth retrievals (A. Kuciauskas et al., Validation and application of satellite-derived aerosol optical depth algorithm during the United Arab Emirates Unified Aerosol Experiment (UAE^2), manuscript in preparation, 2008).

The boundary layer is lower by ~300 m. In the lowest levels, ω_v values are double those at MAARCO. Dust concentrations are also higher in the marine boundary layer (MBL). A significant pollution layer with peak concentrations of 15 μg m^{-3} was observed just above the MBL. Examination of the COAMPS® wind fields for 8 September (Figure 5g), shows that although the distance along the flight path from MAARCO to Sir bu Nair Island is 80 km, the sampled air mass has a substantial alongshore trajectory. Hence, even though the distance between the two sites is relatively short, the time spent over water for the two air masses is significantly different (over 12 h). The flow field also explains the pollution plume aloft over Sir Bu Nair Island, as the trajectories place it over the offshore petroleum processing facilities with active flaring activity west of Abu Dhabi.

5. Case Studies of Significant Aerosol Events

[38] During the UAE^2 field campaign three key aerosol events occurred which give insight into the dynamics of aerosol particles in the AG region: (1) the significant pollution event of 30 August; (2) the Shamal dust event of 12 September 2004 which brought the highest dust concentrations to the SAG; and (3) a 29 September offshore flow event when the aircraft track followed the wind direction from 80 km inland out to Sir bu Nair Island, 80 km offshore.

5.1. The 30 August to 1 September 2004 Pollution Event

[39] Average fine mode mass concentrations at the MAARCO site for the 30 August to 1 September event were above 100 μg m^{-3}, the highest pollution levels measured during the UAE^2 mission. Conversely, dust concentrations and coarse mode AOT fractions were at the near the lowest values measured during the UAE^2 mission. On the basis of the analysis of AERONET data by *Eck et al.* [2008] and the data corresponding to the profile in Table 1, fine mode particles contributed more than 75% of the total 500 nm optical depth of ~0.6. The sources of these particles are the multitude of offshore and island based petroleum extraction and processing facilities that commonly flare waste gas.

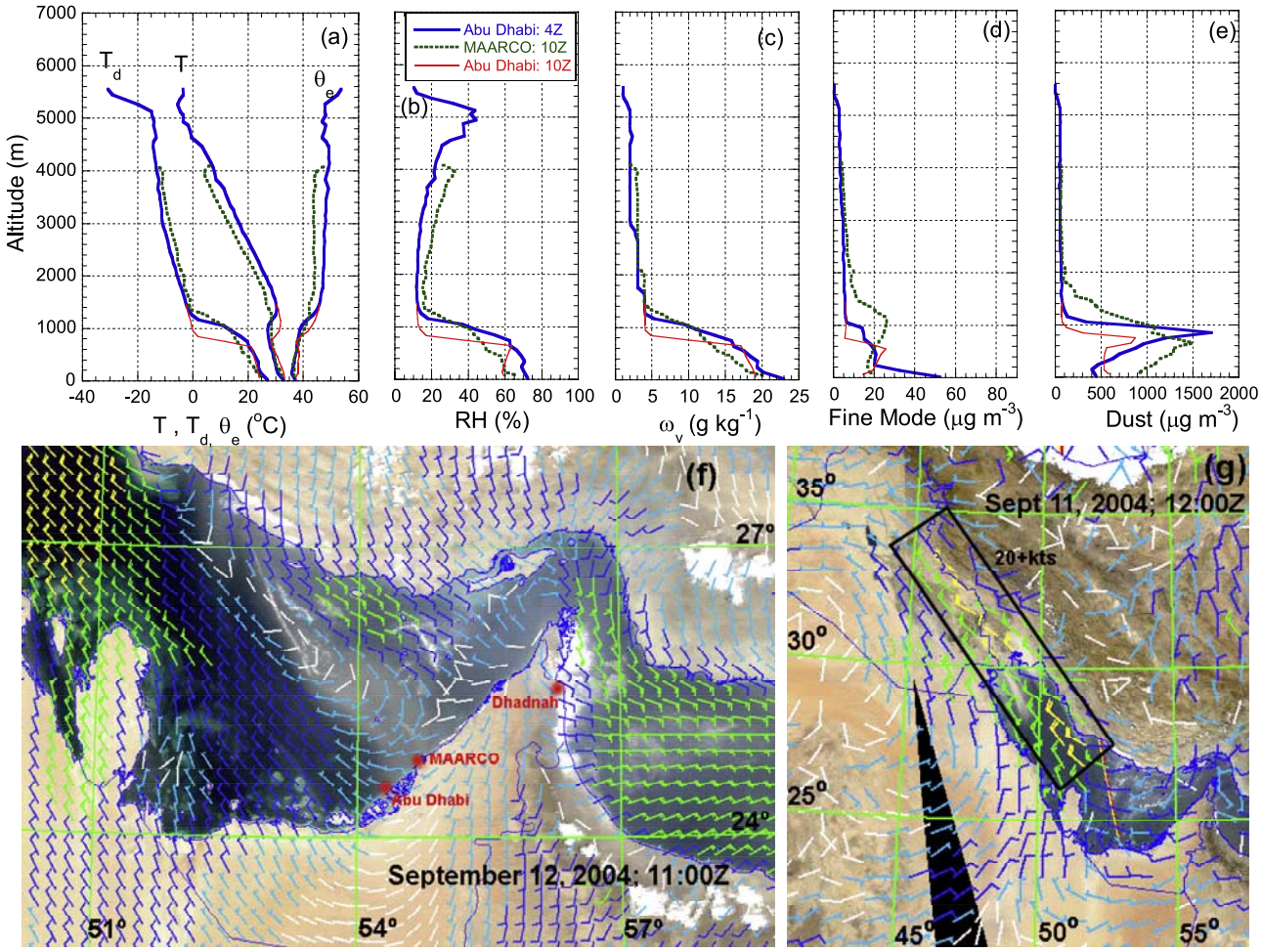

Figure 7. (a–f) Same format as Figure 5 for the dust event from Iraq on 12 September 2004. (g) MODIS RGB and COAMPS® surface wind fields for the origin of the dust plume on 11 September 2004.

[40] During this period, a single flight was conducted on 30 August. A summary of related aircraft, model and remote sensing data is presented in Figure 6. The vertical profiles of state variables and aerosols have characteristics unusual for NW flow conditions. From Abu Dhabi radiosonde data the bottom of the subsidence inversion began at 6000 m. It was the highest subsidence inversion during the mission, and was above the Aerocommander profile maximum altitude for that flight. Just underneath the subsidence inversion, a sporadic altocumulus deck was present. Midlevel moisture was present from 3500 to 6000 m. Near the surface, a shallow stable MBL with strong inversion was present (>4°C), no more than a few hundred meters deep. Pollution concentrations were high within the MBL, with a profile maximum of 90 μg m^{-3} near the surface, and with values as 120 90 μg m^{-3} measured further out to sea. Humidity was also high, with mixing ratios in excess of 22 g kg^{-1} and RH near 80%. On the basis of the surface measurements, these conditions persisted through 1 September. The event began with the weakening of the subtropical high over the Saudi Peninsula on 25–28 August which led to the SW flow conditions described in section 4.3. This reduced the surface wind speeds over the Arabian Gulf region. As a consequence, air remained over the middle of the AG, pollution accumulated from the many active sources and a thick pollution layer developed, as is evident in the high-resolution MODIS optical depth retrievals for 27–30 August (Figure 6g). The low 250 m MBL height also likely trapped pollution nearer to the surface, further increasing concentrations. The low dust concentrations are a result of light regional winds with few stations reporting dust activity near the SAG.

5.2. The 12 September 2004 Shamal

[41] The most dramatic dust event during the UAE^2 mission was the 12 September Shamal that originated in the Tigris-Euphrates basin of Iraq on 11 September. The combination of a midlatitude trough moving eastward over the Black Sea and an intensification of the Indian Monsoonal Trough resulted in strong northwesterly winds over the Tigris-Euphrates valley mobilizing dust from this region. As a result on 12 September instantaneous dust concentrations of 1000 μg m^{-3} and 24 h average values of 300 μg m^{-3} were measured at MAARCO. Midvisible AOTs at MAARCO reached 0.9 (Table 1). In a format similar to Figure 5, aircraft soundings along the UAE coast for this event are presented in Figures 7a–7e. Figures 7f and 7g give the regional satellite imagery, with surface COAMPS®

wind vectors superimposed, for 12 and 11 September, respectively. This flight originally targeted the Dhadnah AERONET site, to support a MISR overpass. As a result, only three vertical profiles in the vicinity of the dust plume were obtained: during morning take off (~0400 UTC); during the decent on the return flight over MAARCO (~1000 UTC); and on a third partial climb just west of Abu Dhabi (1000 UTC).

[42] Like the 30 August pollution event, this case also represents an extreme. Whereas the 30 August event exhibited a very shallow MBL (250 m), the 12 September Shamal showed the deepest (1 km) MBL. Rather than being well mixed, as in the 1 September, 2 October, 3 October, 4 October, and 30 August NW flow events, this Shamal event shows clear dust stratification, with a maximum dust concentration right at the top of the MBL. This appears to be consistent throughout this dust plume, as measurements were made at the leading edge in the morning (0400 UTC), and in the middle (MAARCO) and back (Abu Dhabi) edge in the early afternoon (1000 UTC). In all three profiles, very little dust was sampled above the MBL inversion. From Figure 7d pollution concentrations are highest near the surface in the morning (likely from local sources) and 6 h later are found at the top of the inversion over MAARCO and Abu Dhabi. Dust concentrations decreased by half within the 6 h time frame of the two Abu Dhabi profiles. The satellite image in Figure 7f taken 1 h after landing, shows that Abu Dhabi was situated on the back edge of the dust plume that covered the eastern half of the SAG. This provides a pictorial explanation of the decreased dust concentrations between the two profiles.

5.3. The 29 September Offshore Flow Land Breeze Event

[43] Coastal sea breeze phenomenon can be observed on most days of the year over the entire AG coastline [*Zhu and Atkinson*, 2004]. The land/sea breeze adds significant complexity to the coastal flow patterns, which we believe ultimately influence much of the aerosol vertical distribution. A discussion of the land/sea breeze climatology, and model simulations of the SAG during UAE^2 can be found in *Eager et al.* [2007, 2008]. For the case presented here, offshore flow developed at night in response to a pressure gradient between the cooler land surface (26–29°C) and the warmer AG water (~30°C). A weak line of convective clouds develops over a vertical circulation 20 to 100 km offshore, with return air above the boundary layer advected inland. This phenomenon can be observed on most days of the year over the entire AG coastline [*Zhu and Atkinson*, 2004].

[44] To provide an example of how an offshore land breeze can impact the vertical distribution of thermodynamic and aerosol properties, the data from a land breeze flight conducted the morning of 29 September 2004 are presented. The first profile began at 0800 LST over the Al Khaznah AERONET site roughly 50 km inland, and progressed out toward Sir bu Nair Island (Figure 2) 80 km offshore. Longitudinal cross sections of potential temperature (θ), ω_v, and inferred dust concentration (c_m, μg m^{-3}) are shown in Figures 8a, 8b, and 8c, respectively. The winds were southeasterly and generally along the flight track.

[45] At Al Khaznah we observed the early morning, or nocturnal, 200 m deep stable boundary layer embedded in the previous day's 1200 m deep boundary layer. The stable surface layer was slightly enriched in water vapor and contained high concentrations of dust (700 μg m^{-3}) trapped within the nocturnal boundary layer. As the flight moved toward the coast, a decrease in θ between Al Khaznah and the coast coincided with an increase in ω_v that was the likely remnants of the previous day's sea breeze. Aircraft readings measured 7 m s^{-1} at the coast with dust concentrations of 1000 μg m^{-3}. The surface layer was clearly visible over MAARCO as a peak in dust concentrations.

[46] As the air mass moved from the shore out to sea, we saw a marked increase in ω_v in the lowest layers, due to latent heat flux. For land breeze conditions, the air is slightly cooler than the water, so the atmosphere is weakly unstable. However, dust, water vapor, and temperature remain poorly mixed behind the land breeze front. In flight, we identified the front by thin band of clouds normal to the prevailing wind direction that formed a minor convergence zone at the land breeze front. These clouds appear in the "dust" concentration plot (Figure 8c) as red data points at 54.3 E longitude and 500 m altitude. Such clouds were commonplace during the mission and were frequently used to determine the location of the land breeze front.

[47] At the vicinity of the front, the vertical gradients were eliminated by turbulent mixing (as detected on the aircraft) from both below (slightly unstable) and above (cloud convection), along with the large-scale lifting (~1 m s^{-1}) of (as estimated from aircraft winds). Because the mean flow was out into the gulf, the net impact of this land breeze was to form low-level peaks in dust concentrations nearshore, and eventually move dust and moisture upward at the front. Mesoscale processes such as these contributed to the complicated vertical distributions observed over the SAG during UAE^2.

6. Discussion and Conclusions

[48] During UAE^2 the Aerocommander 690A collected a large and diverse data set over the SAG and UAE. To our knowledge, complete information on meteorology coupled with aerosol particle profiles of very high pollution and dust concentration events has never been reported in the literature for this region.

[49] In this paper, representative cases are presented in detail to familiarize the reader to the aircraft observations taken during UAE^2 and to summarize the thermodynamic and aerosol vertical distributions observed during the campaign. Our findings support those of other UAE^2 papers which show the SAG is a highly complicated mix of fine mode pollution from the region's major petrochemical industries and cities, and coarse mode dust from local and long-range sources. Dust and pollution can be found above, below or through the strong thermodynamic inversions present over the SAG. On the basis of our data, and the many references throughout this manuscript, we have identified several processes controlling thermodynamic and aerosol vertical distribution.

[50] 1. Deep, well mixed, and dust laden daytime boundary layers form over the interior deserts and advect over the cooler AG waters, moist stable internal boundary layers

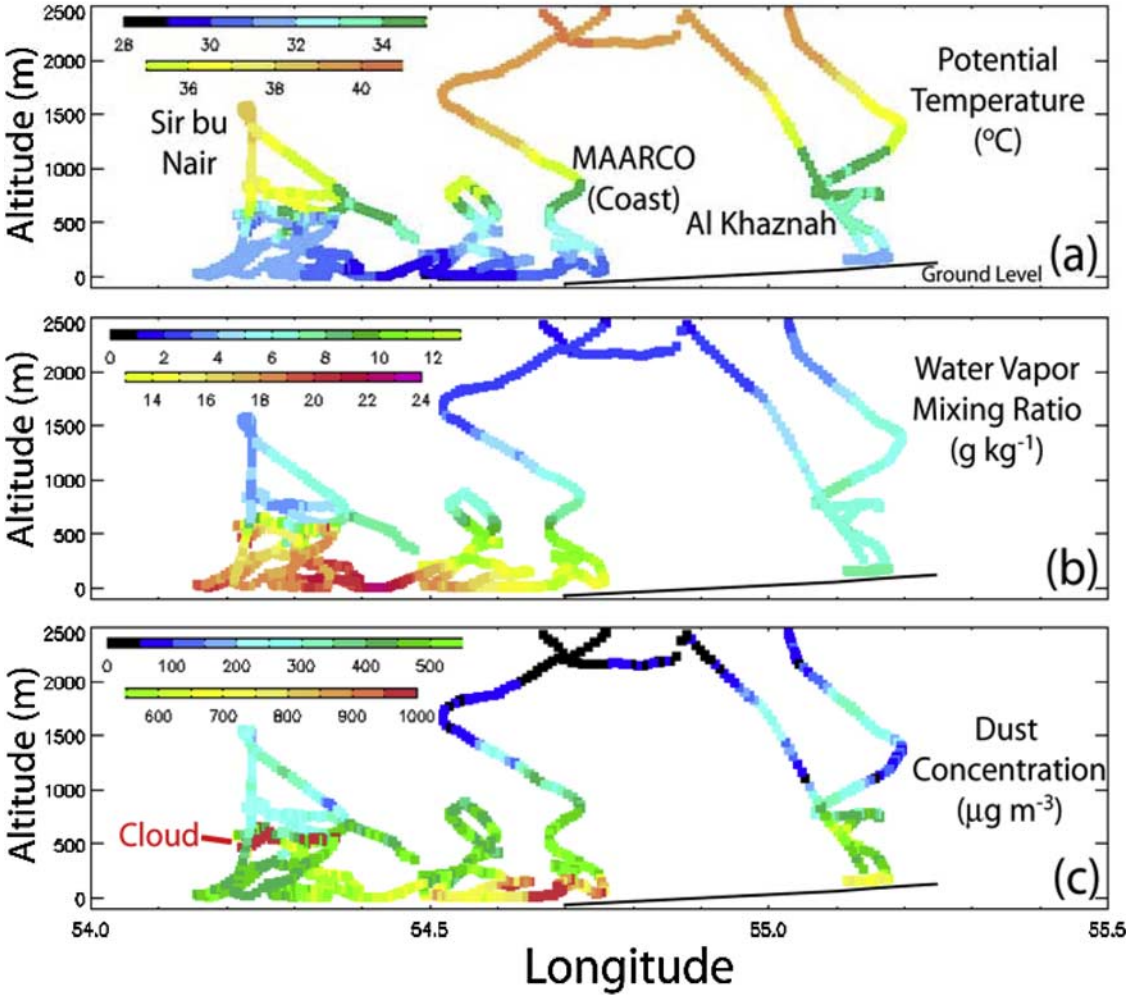

Figure 8. Flight track longitudinal cross sections of (a) potential temperature, θ, in °C; (b) water vapor mixing ratio, ω_v, in g kg^{-1}; and (c) estimated dust concentration, c_v, in μg m^{-3}. These are for (a–c) the 1440–1746 LST 2 October sea breeze and (d–f) the 0645–1005 LST 29 September land breeze flights.

quickly develop into a marine boundary layer (MBL), decoupling the dry dust laden air aloft from the moist aerosol laden air below. In such cases, dust can appear uniform in concentration across an MBL inversion.

[51] 2. A near surface dust layer is formed over the SAG when dust laden airflows out over the water in the nocturnal land breeze. If air is advecting from the land over the AG in a nighttime boundary layer, dust produced during the night or residual dust from the previous day will be injected over the water at low levels beneath the MBL that later forms. This results in an over-water dust layer near the surface.

[52] 3. Unlike dust, pollution has both land based and island sources via urban and petrochemical emissions, respectively. If flare buoyancy is strong enough, isolated plumes form above the already established MBL. If not, pollution is trapped below.

[53] 4. This unique data set with aircraft, ground based, and satellite data captured the littoral complexities of the SAG. Examples of coastal flows, land/sea breezes and pollution events were sampled and measured. With this unique data set, a secondary set of data evaluation and model simulations for the UAE^2 campaign are underway to propagate uncertainties into large-scale modes, remote sensing, and chemistry.

Appendix A: Overview of 690A Aerocommander and Cheyenne II Aircraft

[54] Two aircraft were employed for the UAE^2 campaign: a pressurized 690A Aerocommander and an unpressurized Piper Cheyenne II (T1040). These aircraft were shared with an ongoing cloud and precipitation research project operated by NCAR for the UAE Dept. of Water Resource Studies. The 690A is a well developed research aircraft which has seen much cloud, aerosol and chemistry service with the South African Meteorological Service and the University of Witwatersrand. Its configuration with six available PMS canisters, an aerosol inlet, and numerous port openings was optimized for combined cloud and aerosol research. Nominally an 8 seat aircraft, the 690A is pressurized and reached altitudes of over 6 km (500 hPa) during the mission.

[55] Table A1 lists included instrumentation for the mission. The bulk of the instrumentation on the 690A is commonly utilized by research aircraft. Trimble GPS

Table A1. Instrumentation on the Aerocommander 690A

Variable	Instrument and Manufacturer	Uncertainty and Availability
Cabin		
GPS navigation	Garmin GNS 430	30 m, all
Aircraft attitude	Aventech AIMS differential GPS	<±0.3, 0.3, 0.5° PRA, available after 12 Sep
Aerosol backscatter	Porter LIDAR	see text, 2–25 Sep
Light scattering	TSI 3-λ nephelometer	<0.02 km^{-1} total scattering only
Coarse mode sizer	TSI APS 3321	see text, all
SO_2	thermal SO_2	<1 ppm, available after 1 Oct
Aerosol particle composition	filters for XRF and IC	see Reid et al. (manuscript in preparation, 2008), all
Hyperspectral radiance	ASD Fieldspec	see text; available after 1 Oct
Skin		
Temperature	Rosemount total temperature	<0.3 K all
Temperature	Vaisala Humicap total temperature	<0.4 K all
Humidity	EGG chilled mirror dew point	<0.5 K, all
Humidity	Vaisala Humicap RH	<5% RH, all
Static and dynamic pressure	Rosemont Pressure Probe	~ 0.1 hPa, all
Sea surface temperature	Heitronics KT19 IR thermometer	<0.3 K, all
Up and down solar radiometers	Kipp and Zonen	<2%, all
Cloud liquid water	King Probe	<0.1 g m^{-3}, all
PMS Cans		
Fine mode sizer	DMT PCASP	see text, all
Coarse mode sizer	DMT FSSP (high gain)	see text, all
Cloud droplet sizer	PMS FSSP (low gain)	see text and *Bruintjes et al.* [2005], all
Cloud droplet sizer	PMS FSSP (low gain, backup)	see text and see *Bruintjes et al.* [2005], all
Small precipitation	PMS 1-D probe	see *Bruintjes et al.* [2005], all
Large precipitation	PMS 2-D probe	see *Bruintjes et al.* [2005], all

system, Vaisala combined temperature and humidity probe, EGG-dew point hygrometer, Kipp and Zonen Radiometers and a large collection of DMT and PMS probes. Details on most of these instruments and their calibration are given by *Reid et al.* [2003b]. However, there are a number of issues that require expanded explanation.

[56] First, navigational data (latitude, longitude, and altitude) were provided throughout the mission by a Garmin GNS 430. For flights after 12 September, an additional Aventech AIMS differential GPS system was installed which provided pitch, roll and azimuth to ±0.3, ±0.3 and ±0.5° uncertainty, respectively.

[57] The 690A carries up to 6 PMS cans (two on each wing plus two on the nose). Included during the mission for cloud measurements were two FSSP-100s, a PMS 1-D probe and a PMS 2-D probe. The PCASP and one of the FSSPs were DMT modified (SPP 200 and 100, respectively). The PCASP in particular has proven itself the most useful in our analysis of pollution and dust vertical profile during the UAE^2 mission, and we rely heavily on it in our analyses. The PCASP was operated with deicing heaters on, resulting in a dry size distribution even under moist conditions [*Reid et al.*, 2006]. With a size range from 0.1 to 3.0 μm for a nominal index of refraction of 1.58, the PCASP can resolve nearly all of the fine mode pollution mass, as well as most of the common mode dust's optically active particles. Frequent calibrations checks during the mission found that the PCASP calibration stayed within DMT factory setting.

[58] Cabin instrumentation was fed by a scaled down inlet system modeled on the CIRPAS Twin Otter [*Hegg et al.*, 2005]. This inlet fed a TSI APS 3321, a TSI 3 λ nephelometer, a filter sampler and, for the last few flights, a Thermo SO_2 instrument. While Hegg et al. found that the aerodynamic cut point for this inlet is approx. Five μm, in the exact configuration in scaled down version and plumbing on the 690A we found it to be closer to 2.5 μm. Because of an instrumentation error, the 3-λ nephelometer could only measure total scattering (backscatter shutter was inoperable). Filter samples taken included Teflon filters for X-Ray Florescence (XRF) analysis at the Desert Research Institute (DRI) aerosol laboratory, and polycarbonates for Scanning Electron Microscopy (SEM) and absorption analysis. Details on particle chemistry are given by E. A. Reid et al. (Chemical and morphological properties of southwest Asian dust, manuscript in preparation, 2008).

[59] The last major modification to the 690A was placement of a 40 cm port on the starboard size of the aircraft to house the University of Hawaii lidar system, [*Porter et al.*, 2002]. This configuration allowed it to be pointed either upward or downward, depending on the aircraft altitude. On select occasions, when the plane was flying level in an aerosol layer, the lidar was pointed forward. These forward looking lidar measurements allowed for the testing of a new lidar approach to derive quantitative aerosol extinction values [*Porter et al.*, 2007]. In order to make the system eye safe (at greater than 200 m range), a diverging laser beam was used, combined with a nonimaging optics approach to collect the light. In this configuration the system had a range of 60–5000 m. The system operated on approximately 1/3 of the flights.

[60] On the last 4 flights of the mission, the lidar was replaced with an Analytical Spectral Devices (ASD) Fieldspec spectrometer to measure the hyper spectral signatures of the various soil regimes in the region. This instrument operated with a spectral range of 350–250 nm at 3 to 10 nm resolution and a 2° field of view. Noise equivalent radiances are at 1.4×10^{-9}, 1.4×10^{-9}, and 1.4×10^{-9} W cm^{-2} nm^{-1} sr^{-1} at 700, 1400 and 2100 nm, respectively.

[61] Also operating in the area was the Orsmond Aviation Piper Cheyenne II aircraft. Equipped for a concurrent cloud seeding experiment, it was only equipped for navigation and state variables such as pressure (Rosemount), temperature and relative humidity (Vaisala). Flying predominately out of Al Ain airport, it provided mission investigators with basic thermodynamic soundings. Being unpressurized, this aircraft was also used on three occasions to collect Microtops handheld Sun photometer data through the starboard window (340, 440, 500, 875 nm, and 970 nm water vapor). On the basis of the study and protocols of *Ichoku et al.* [2002], *Porter et al.* [2007] and our own analysis, we expect in flight optical depths to be within ±0.05.

[62] **Acknowledgments.** The UAE^2 mission required the help and assistance of a number of individuals from all of the participating organizations as listed in the author list. Particular thanks are to the staff of the Department of Water Resource Studies (DAS) and the South African air and maintenance crews. We also thank several individuals with their help in the postanalysis paper including Elizabeth Reid and Cynthia Curtis. This research was supported by the Office of Naval Research Code 32 and 35 and the NASA Radiation Sciences Program. Flight hours were provided by the Naval Research Laboratory platform support fund and the UAE DAS. The work of R. Kahn is supported by NASA's Climate and Radiation program, Atmospheric Composition Research and Analysis Programs, and the EOS-MISR instrument project.

References

Ackerman, S. A., and S. K. Cox (1982), The Saudi Arabian Heat Low: Aerosol distribution and thermodynamic structure, *J. Geophys. Res.*, *87*, 8991–9002, doi:10.1029/JC087iC11p08991.

Ackerman, S. A., and S. K. Cox (1989), Surface weather observations of atmospheric dust over the southwest summer monsoon region, *Meteorol. Atmos. Phys.*, *41*, 19–34, doi:10.1007/BF01032587.

Alpert, P., P. Kishcha, A. Shtivelman, S. O. Krichak, and J. H. Joseph (2004), Vertical distribution of Saharan dust based on 2.5-year model predictions, *Atmos. Res.*, *70*(2), 109–130, doi:10.1016/j.atmosres.2003.11.001.

Atkinson, B. W., J. G. Li, and R. S. Plant (2001), Numerical modeling of the propagation environment in the atmospheric boundary layer, *J. Appl. Meteorol.*, *40*, 586–603, doi:10.1175/1520-0450(2001)040<0586:NMOTPE>2.0.CO;2.

Brooks, I. A., and D. P. Rogers (2000), Aircraft observations of the mean and turbulent structure of a shallow boundary layer over the Persian Gulf, *Boundary Layer Meteorol.*, *95*, 189–210, doi:10.1023/A:1002623712237.

Bruintjes, R. T., T. Jensen, D. Breed, V. Salazar, S. Piketh, K. Ross, A. Al Mandoos, and A. Al Mangoosh (2005), Observed cloud microphysical characteristics in India and the Arabian Peninsula: High droplet concentrations does not always retard coalescence, *Eos Trans. AGU*, *86*(52), Fall Meet. Suppl., Abstract A44A-3.

Draxler, R. R., and G. D. Hess (1997), Description of the Hysplit_4 modeling system, *NOAA Tech. Memo.*, *ERL ARL-224*, 24 pp., NOAA, Silver Spring, Md., Dec.

Eager, R. E., et al. (2007), A seasonal statistical evaluation of COAMPS over the Arabian Gulf region, *Pure Appl. Geophys.*, *164*, 1746–1747, doi:10.1007/s00024-007-0229-0.

Eager, R. E., S. Raman, A. Al Mandoos, D. L. Westphal, and J. S. Reid (2008), A climatology study of the sea and land breezes in the Arabian Gulf region, *J. Geophys. Res.*, doi:10.1029/2007JD009710, in press.

Eck, T. F., et al. (2008), Spatial and temporal variability of column integrated aerosol optical properties in the southern Arabian Gulf and United Arab Emirates in summer, *J. Geophys. Res.*, *113*, D01204, doi:10.1029/2007JD008944.

Hegg, D. A., D. S. Covert, H. Jonsson, and P. A. Covert (2005), Determination of the transmission efficiency of an aircraft aerosol inlet, *Aerosol Sci. Technol.*, *39*, 966–971, doi:10.1080/02786820500377814.

Heishman, J. (1999), *Commanding Officer, Forecaster's Handbook*, U.S. Navy Cent. Meteorol. and Oceanogr. Cent., Manama, Bahrain.

Ichoku, C., R. Levy, Y. J. Kaufman, L. A. Remer, R. R. Li, V. J. Martins, B. N. Holben, N. Abuhassan, I. Slutsker, T. F. Eck, and C. Pietras (2002), Analysis of the performance characteristics of the five-channel Microtops II Sun photometer for measuring aerosol optical thickness and precipitable water vapor, *J. Geophys. Res.*, *107*(D13), 4179, doi:10.1029/2001JD001302.

Middleton, N. J. (1986), A geography of dust storms in south-west Asia, *Int. J. Climatol.*, *6*, 183–196, doi:10.1002/joc.3370060207.

O'Neill, N. T., T. F. Eck, B. N. Holben, A. Smirnov, O. Dubovik, and A. Royer (2001), Bimodal size distribution influences on the variation of Angstrom derivatives in spectral and optical depth space, *J. Geophys. Res.*, *106*, 9787–9806, doi:10.1029/2000JD900245.

Porter, J. N., B. Lienert, S. K. Sharma, and H. W. Hubble (2002), A small portable Mie-Rayleigh lidar system to measure aerosol optical and spatial properties, *J. Atmos. Oceanic Technol.*, *19*, 1873–1877, doi:10.1175/1520-0426(2002)019<1873:ASPMRL>2.0.CO;2.

Porter, J. N., T. A. Clarke, J. S. Reid, G. Shaw, H. Maring, E. A. Reid, D. Kress, and B. Lienert (2007), Hand held Sun photometer measurements from small aircraft, *J. Atmos. Oceanic Technol.*, *24*, 1588–1597, doi:10.1175/JTECH2087.1.

Prospero, J. M., et al. (2002), Environmental characterization of global sources of atmospheric soil dust identified with the Nimbus 7 total ozone mapping spectrometer (TOMS) absorbing aerosol product, *Rev. Geophys.*, *40*(1), 1002, doi:10.1029/2000RG000095.

Rao, P. G., H. R. Hatwar, M. H. Al Sulaiti, and A. H. Al Mulla (2003), Summer shamals over the Arabian Gulf, *Weather*, *58*, 471–478, doi:10.1256/wea.282.02.

Reid, J. S., et al. (2003a), Analysis of measurements of Saharan dust by airborne and ground-based remote sensing methods during the Puerto Rico Dust Experiment (PRIDE), *J. Geophys. Res.*, *108*(D19), 8586, doi:10.1029/2002JD002493.

Reid, J. S., H. H. Jonsson, H. B. Maring, A. A. Smirnov, D. L. Savoie, S. S. Cliff, E. A. Reid, M. M. Meier, O. Dubovik, and S.-C. Tsay (2003b), Comparison of size and morphological measurements of coarse mode dust particles from Africa, *J. Geophys. Res.*, *108*(D19), 8593, doi:10.1029/2002JD002485.

Reid, J. S., B. Brooks, K. K. Crahan, D. A. Hegg, T. F. Eck, N. O'Neill, G. de Leeuw, E. A. Reid, and K. D. Anderson (2006), Reconciliation of coarse mode sea-salt aerosol particle size measurements and parameterizations at a subtropical ocean receptor site, *J. Geophys. Res.*, *111*, D02202, doi:10.1029/2005JD006200.

Reid, J. S., E. A. Reid, S. J. Piketh, S. A. Cliff, A. Al Mandoos, A. L. Walker, and S.-C. Tsay (2008), Dynamics of southwest Asian dust particle size characteristics with implications for global dust research, *J. Geophys. Res.*, doi:10.1029/2007JD009752, in press.

Smirnov, A., B. N. Holben, O. Dubovik, N. T. O'Neill, T. F. Eck, D. L. Westphal, A. K. Goroch, C. Pietras, and I. Slutsker (2002), Atmospheric aerosol optical properties in the Persian Gulf region, *J. Atmos. Sci.*, *59*, 620–634, doi:10.1175/1520-0469(2002)059<0620:AAOPIT>2.0.CO;2.

Strapp, J. W., W. R. Leaitch, and P. S. K. Liu (1992), Hydrated and dried aerosol-size distribution measurements from the particle measuring systems FSSP-300 probe and the deiced PSASP-100X probe, *J. Atmos. Oceanic Technol.*, *9*, 548–555, doi:10.1175/1520-0426(1992)009<0548:HADASD>2.0.CO;2.

Warner, T. T. (2004), *Desert Meteorology*, Cambridge Univ. Press, Cambridge, U. K.

Warner, T. T., and R. S. Sheu (2000), Multiscale local forcing of the Arabian Desert daytime boundary layer, and implications for the dispersion of surface released contaminants, *J. Appl. Meteorol.*, *39*, 686–707, doi:10.1175/1520-0450(2000)039<0686:MLFOTA>2.0.CO;2.

Zhu, M., and B. W. Atkinson (2004), Observed and modeled climatology of the land-sea breeze circulation over the Persian Gulf, *Int. J. Climatol.*, *24*, 883–905, doi:10.1002/joc.1045.

A. Al Mandoos and A. Al Mangoosh, Department of Atmospheric Studies, Ministry of Presidential Affairs, P.O. Box 4815, Abu Dhabi, United Arab Emirates.

R. T. Bruintjes and T. L. Jensen, National Center for Atmospheric Research, Boulder, CO 80307, USA.

R. P. Burger, S. J. Piketh, and K. E. Ross, Climatology Research Group, University of Witwatersrand, Private Bag 2050, WITS 2050, Johannesburg, South Africa.

B. N. Holben, C. Hsu, R. A. Kahn, and S.-C. Tsay, NASA Goddard Space Flight Center, Code 614.4, Greenbelt, MD 20771, USA.

A. P. Kuciauskas, E. A. Reid, J. S. Reid, A. L. Walker, and D. L. Westphal, Marine Meteorology Division, Naval Research Laboratory, 7 Grace Hopper Avenue, Stop 2, Monterey, CA 93943-5502, USA. (reidj@nrlmry.navy.mil)

S. D. Miller, Cooperative Institute for Research in the Atmosphere, Colorado State University, Fort Collins, CO 80523, USA.

J. N. Porter, School of Ocean and Earth Science and Technology, University of Hawai'i, 2525 Correa Road, HIG Room 313, Honolulu, HI 96822, USA.